Thesis for the Degree of
Master of Education

Structure and Properties of Silver(II) Complexes with Macrocyclic Ligand

by

Ja Ran Moon

Graduate School of Education

Pukyong National University

August 2010

Structure and Properties of Silver(II) Complexes with Macrocyclic Ligand

거대고리 은(II) 착화합물의 구조와 특성

Advisor : Prof. Ju Chang Kim

by
Ja Ran Moon

A thesis submitted in partial fulfillment of the requirement
for the degree of

Master of Education

Graduate School of Education
Pukyong National University

August 2010

Structure and Properties of Silver(II) Complexes with Macrocyclic Ligand

A dissertation

by

Ja Ran Moon

Approved by:

_____

Chairman: Sang Yong Pyun

_____ _____

Member: Yong-Cheol Kang Member: Ju Chang Kim

August 25, 2010

Table of Contents

List of Tables

List of Figures

Structure and Properties of Silver(II) Complexes with Macrocyclic Ligand

문 자 란

부경대학교 교육대학원 화학교육전공

요 약

새로운 은(II) 착화합물인 $\{[Ag(\mathbf{L1})](NO_3)_2 \cdot 4H_2O\}_n$ (**1**)과 $\{[Ag(\mathbf{L2})](NO_3)_2 \cdot 2H_2O\}_n$ (**2**) (**L** = 3,14-dimethyl 2,6,13,17-tetraazatricyclo[14,4,$0^{1.18}$,$0^{7.12}$] docosane) 을 합성하였고, 원소분석, 분광학, 전기화학적 분석 및 X-ray 회절법 등의 분석을 통해 구조적인 특성을 확인 할 수 있었다. 첫 번째 착화합물인 $\{[Ag(\mathbf{L1})](NO_3)_2 \cdot 4H_2O\}_n$ (**1**)은 거대고리 리간드에 미리 자리잡고 있는 N-H 작용기와 질산 이온간의 수소결합에 의해서 1D 초분자 사슬 구조를 형성하고, 각각의 1D 사슬은 격자 내의 물 분자와의 수소결합에 의해서 2D 평면 구조를 형성하였다. 두 번째 착화합물인 $\{[Ag(\mathbf{L2})](NO_3)_2 \cdot 2H_2O\}_n$ (**2**)는 *cis* 형태로 cyclohexane 고리가 융합된 거대고리 리간드를 가지고 있으며, 수소결합으로 연결된 거대고리 리간드의 N-H 작용기와 질산이온을 격자 내 물 분자가 연결해 줌으로써 1D 초분자 사슬을 형성한다. 거대고리 리간드의 경직성과 입체장애가 구조적인 기하구조를 결정하는데 중요한 역할을 한다는 것을 알 수 있었다.

Structure and Properties of Silver(II) Complexes with Macrocyclic Ligand

Abstract

Two new silver(II) complexes, $\{[Ag(\mathbf{L1})](NO_3)_2 \cdot 4H_2O\}_n$ **(1)** and $\{[Ag(\mathbf{L2})](NO_3)_2 \cdot 2H_2O\}_n$ **(2)** (**L** = 3,14-dimethyl 2,6,13,17-tetraazatricyclo[14,4,$0^{1.18}$,$0^{7.12}$] docosane) have been synthesized and structurally characterized by a combination of analytical, spectroscopic, electrochemical and X-ray diffraction methods. The complex **1** exhibits a 1D supramolecular polymer with silver(II) macrocycle **L1** and nitrate ions, where 1D chain is formed by hydrogen bonds between the two sets of pre-organized N-H groups of the macrocycle and nitrate ions. The lattice water molecules mediate to interconnect each 1D chain to form the 2D supramolecular sheet. The complex **2** exhibits a 1D supramolecular polymer with silver(II) macrocycle **L2**, nitrate ions and lattice water molecules. The 1D chain of complex **2** is formed by hydrogen bonds between the nitrate ions and lattice water molecules. In **1** and **2** the unusual high oxidation state of Ag(II) is stabilized by the macrocycles **L1** and **L2**.

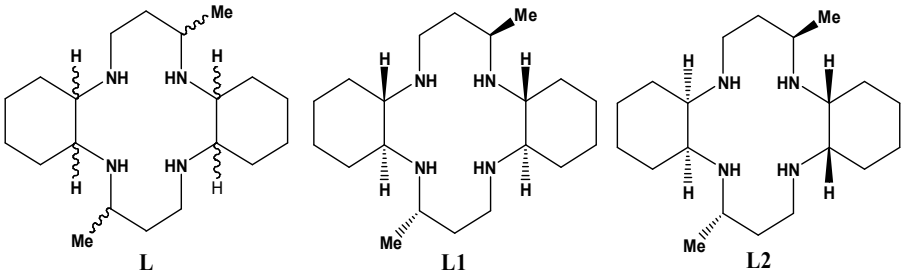

Introduction

Transition metal complexes with synthetic tetraazamacrocycles have been of great interest in recent years not only due to their versatile applications but also for the usefulness in elucidating structure-reactivity relationship [4]. One of the distinctive features of tetraazamacrocycles is their ability to stabilize metal ions in high oxidation states. This is especially true in the chemistry of Ag(II) ions. A Ag(II) ion is usually difficult to exist because it is unstable at room temperature. The Ag(II) ions in the high oxidation state are stable when they are coordinated to N-donor lignads [6-13].

Complexes **1** and **2** contain unusual high oxidation state of Ag(II) ions which are stabilized by macrocyclic ligands **L1** and **L2**, respectively. The complexes are the product of disproportionation of the Ag(I) complex according to the following equation:

$$2Ag(I) + \mathbf{L} \rightarrow Ag(II)\mathbf{L} + Ag \downarrow$$

It has generally been understood that the macrocyclic ligands possessing a suitable cavity size and hard nitrogen donor atoms can form stable Ag(II) complexes in aqueous solution [6,7].

The present tetraazamacrocyclic ligands **L1** and **L2** which are one of the 16 possible diastereoisomers of **L**, respectively, first synthesized by Kang et al [14], have long been used for the preparation of many interesting transition metal complexes [5, 15-17]. The macrocyclic ligand **L** is a derivative of a cyclam, the

macrocycle **L1** has two *trans*-fused cyclohexane rings and the macrocycle **L2** has two *cis*-fused cyclohaxane rings on a cyclam. The ligand skeleton of the complexes adopts typical *trans* III conformation with two gauche five-membered chelate rings and two chair form six-membered rings [22]. As a continuation of the investigation of the transition metal chemistry of **L1** and **L2**, two Ag(II) supramolecular polymers $\{[Ag(\mathbf{L1})](NO_3)_2 \cdot 4H_2O\}_n$ (**1**) and $\{[Ag(\mathbf{L2})](NO_3)_2 \cdot 2H_2O\}_n$ (**2**) in which the high oxidation state of silver is stabilized by the tetraazamacrocycles **L1** and **L2** have been prepared and studied in this thesis. It is expected that the coordination as well as hydrogen bonding environment change between the two isomers by a structural difference. The details of the synthesis, structures, spectroscopic and electrochemical properties of complexes are discussed in this thesis.

Experimental

Physical measurements

All chemicals used in the synthesis were of reagent grade and used without further purification. Distilled water was used for all procedures. Infrared spectra of solid samples were recorded on a Perkin-Elmer Paragon 1000 FT-IR spectrophotometer between 4000 and 400 cm^{-1} as Nujol mulls on KBr discs. UV/vis spectra were measured on a Cary 1C spectrophotometer within the range 200-800 nm. EPR spectra were obtained by a JES PX2300 digital X-band (ν = 9.453 and ν = 9.443 GHz) spectrometer at ambient temperature. Elemental analysis was performed by the Korea Research Institute of Chemical Technology, Daejeon, Korea. The free ligands **L1** and **L2** were prepared according to a literature procedure [14]. Electrochemical measurements were performed in a standard three electrode system with Pt disk working electrode, $Ag/AgNO_3$ (0.01 M) reference electrode and Pt counter electrode using a PAR 263 A potentiostat. The electrolyte solution was 0.1M triethylammonium hexafluorophosphate (TEAP) in dry acetonitrile. The potential scan rate in cyclic voltammetry was 50 mV s^{-1}. The reference potential of $Ag/AgNO_3$ electrode was 0.045 V vs Ferrocene/Ferrocenium potential. The concentration of complexes were not determined

*Synthesis of {[Ag(**L1**)](NO$_3$)$_2$ · 4H$_2$O}$_n$ (**1**)*

To a methanol (10 mL) solution of **L1** (330 mg, 1.0 mmol) was added a water (10 mL) solution of $AgNO_3$ (340 mg, 1.0 mmol). The mixture turned deep orange and metallic silver formed immediately. The metallic silver was filtered off. The orange filtrate was collected and allowed in an open beaker protected from light at ambient temperature. The orange blocks of **1** were obtained in a few weeks. Suitable crystals of **1** for X-ray diffraction studies and other measurements were manually collected under a microscope. Yield > 95%. Anal. Calc. for $C_{20}H_{48}AgN_6O_{10}$: C, 36.06; H, 7.21; N, 12.62; O, 24.04%. Found C, 35.94; H, 7.35; N, 12.44; O, 24.48%. IR (Nujol, cm^{-1}): 3441 (νOH), 3236, 3151 (νNH), 1643 (ν_{as}NOO), 1613 (ν_sNOO).

*Synthesis of {[Ag(**L2**)](NO$_3$)$_2$ · 2H$_2$O}$_n$ (**2**)*

To a methanol (10 mL) solution of **L2** (330 mg, 1.0 mmol) was added a water (10 mL) solution of $AgNO_3$ (340 mg, 1.0 mmol). The mixture turned deep orange and metallic silver formed immediately. The metallic silver was filtered off. The orange filtrate was collected and allowed in an open beaker protected from light at

ambient temperature. The orange blocks of **2** were obtained in a few days. Suitable crystals of **2** for X-ray diffraction studies and other measurements were manually collected under a microscope. Yield > 95%. IR (Nujol, cm^{-1}): 3406 (νOH), 3203 (νNH), 1641 (ν_{as}NOO),

X-ray crystallography

A summary of selected crystallographic data and structure refinement for **1** and **2** is given in Table 1. X-ray data were collected on a Nonius Kappa CCD diffractometer, using graphite monochromated Mo Kα radiation (λ = 0.71073 Å). A combination of 1° ϕ and ω (with κ offsets) scans were used to collect sufficient data. The data frames were integrated and scaled using the Denzo-SMN package [20]. The structures were solved and refined using the SHELXTL\PC V6.1 package [21]. Refinement was performed by full-matrix least squares on F^2 using all data (negative intensities included). Hydrogen atoms were included in calculated positions.

Table 1. Crystal data and structure refinement parameters for [Ag(**L1**)]$(NO_3)_2$ · $4H_2O$ (**1**) and [Ag(**L2**)]$(NO_3)_2$ · $2H_2O$ (**2**)

	1	**2**
Empirical formula	$C_{20}H_{48}AgN_6O_{10}$	$C_{20}H_{44}AgN_6O_8$
Formula weight	640.51	604.48
Temperature (K)	150(1)	150(1)
Crystal system	Triclinic	Triclinic
Space group	Pī	Pī
a (Å)	7.8024(2)	8.5400(4)
b (Å)	8.9087(2)	8.8773(2)
c (Å)	10.6745(3)	9.1096(4)
α (°)	93.9040(12)	72.838(2)
β (°)	105.8290(13)	73.2510(18)
γ (°)	108.8310(12)	77.492(2)
Volume ($Å^3$)	665.63(3)	625.31(4)
Z	1	1
D_{calcd} (Mg/m^3)	1.598	1.605
Absorption coefficient	0.821 mm^{-1}	0.863 mm^{-1}
Crystal size (mm^3)	0.26 x 0.26 x 0.16	0.20 x 0.10 x 0.10
θ range for data collection	2.89 to 27.48°	2.96 to 27.48°
Index range	$-10 \le h \le 9$	$-11 \le h \le 11$
	$-11 \le k \le 11$	$-11 \le k \le 11$
	$-13 \le l \le 13$	$-11 \le l \le 11$
Reflections collected	8056	6601
Independent reflections	3006 [R(int) = 0.0410]	2828 [R(int) = 0.0371]
Completeness to θ	99.3 % (θ = 27.48°)	99.5 % (θ = 25.24°)
Absorption correction	Semi-empirical from equiv.	Semi-empirical from equiv.
Max. and min. transmission	0.883 and 0.800	0.921 and 0.827
Data/restraints/parameters	3006 / 0 / 170	2828 / 0 / 169
Goodness-of-fit on F^2	1.137	1.079
Final R indices [$I>2\sigma(I)$]	R1 = 0.0427	R1 = 0.0322
	wR2 = 0.1260	wR2 = 0.0712
R indices (all data)	R1 = 0.0436	R1 = 0.0356
	wR2 = 0.1268	wR2 = 0.0736
Largest diff. peak and hole	0.756 and -1.067 e. $Å^{-3}$	0.515 and -0.870 e. $Å^{-3}$

Results and Discussion

*Descriptions of structures for **1- 2***

The complex **1,** as illustrated in Figure 1, was obtained by reaction the macrocyclic ligand **L1** and $AgNO_3$ in $MeOH/H_2O$. The coordination environment around the central Ag(II) ion is a square plane with four Ag-N bonds from macrocyclic ligand and two Ag-O bonds from nitrate ions in axial. The silver atom sits on an inversion center. Two weak interactions at the axial sites for the Ag(II) ion have been observed between Ag and O atoms from nitrate ions. The Ag-N distances are in the range of 2.140(2) – 2.150(2) Å. The average distance of Ag-N bond is 2.145(2) Å which agreed with previous reported average of Ag-N bond, in general, which ranges from 2.09 to 2.21 Å [12]. The Ag-O distance of 2.923(2) Å is longer than the corresponding distances ([Ag(**meso-[14]ane**)]$(NO_3)_2$; Ag-O = 2.807(4) Å [12], [Ag(**tmc**)]$(ClO_4)_2$; Ag-O = 2.889(4) Å [13], [Ag(**cyclam**)]$(ClO_4)_2$; Ag-O = 2.788(2) Å [19]; where **meso-[14]ane** = meso-5,5,712,12,14–hexamethyl-1,4,8,11-tetraazacyclotetradecane, **tmc** = 1,4,8,11–tetramethyl-1,4,8,11-tetraazacyclotetradecane, **cyclam** = 1,4,8,11-tetraazacycoltetradecane).

The lattice cell of **1** contains two nitrate ions and four water molecules. The

basic unit [Ag(**L1**)]$(NO_3)_2 \cdot 4H_2O$ works as a "metal complex synthon" for the formation of a 1D supramolecular polymer. Then, the lattice water molecules interconnect each 1D chain through hydrogen bonds to form a 2D supramolecular sheet. As is common, the macrocyclic skeleton in **1** retains the *trans* III conformation with two sets of pre-organized N-H groups which enable to interact with nitrate ions in the proface through hydrogen bonds resulting in the formation of the 1D supramolecular polymer [16].(Figure 2, Table 2).

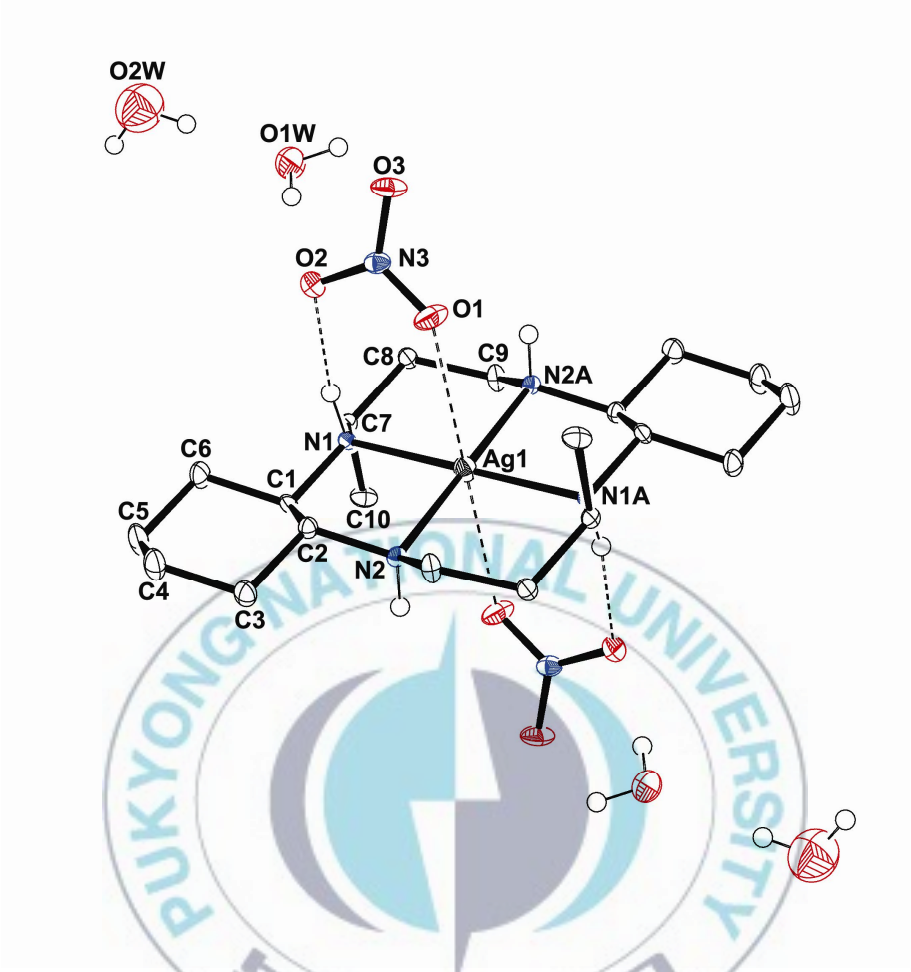

Figure 1. Molecular structure of [Ag(**L1**)]$(NO_3)_2 \cdot 4H_2O$ (**1**) with atom-labeling scheme. Hydrogen atoms other than those participating in hydrogen bonding are omitted for clarity.

(a)

(b)

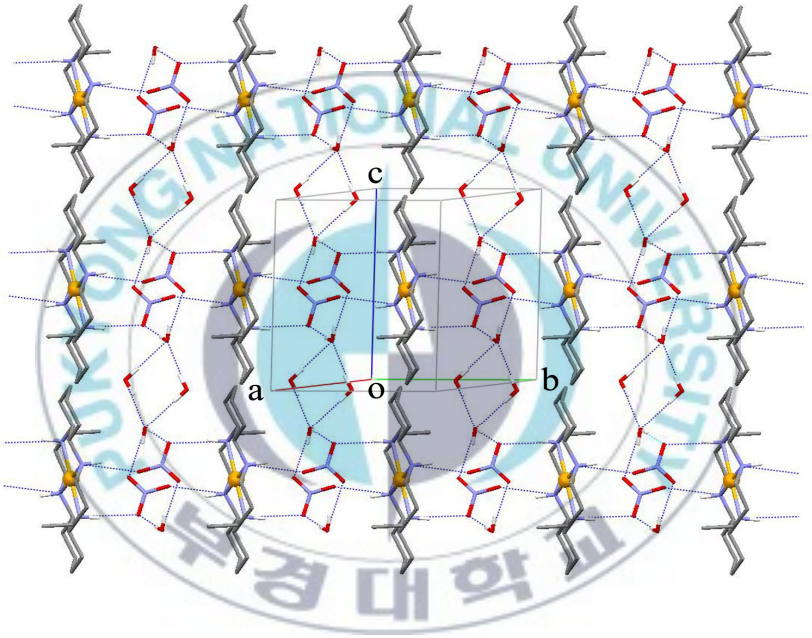

Figure 2. Space-filling (a) and lattice diagram (b) of $\{[Ag(\mathbf{L1})](NO_3)_2 \cdot 4H_2O\}_n$ (**1**) illustrating a 2D supramolecule. Hydrogen atoms are omitted for clarity.

Table 2. Selected bond distances (Å) and angles (°) for [Ag(**L1**)]$(NO_3)_2 \cdot 4H_2O$ (**1**)

Ag1-N1	2.150(2)	Ag1-N2	2.140(2)
Ag1-O1	2.923(2)	O1-N3	1.254(4)
O2-N3	1.258(4)	O3-N3	1.244(3)
N1-Ag1-N2	83.57(9)	N1-Ag1-N2#1	96.43(9)
N1-Ag1-O1	81.32(8)	N2-Ag1-O1	98.55(9)
N1#1-Ag1-O1	98.68(8)	N2#1-Ag1-O1	81.45(9)

Symmetry transformations used to generate equivalent atoms:

#1 -x+1,-y+1,-z+1

Table 3. Hydrogen bonds for [Ag(**L1**)]$(NO_3)_2 \cdot 4H_2O$ (**1**) (Å and °)

D-H···A	d(D-H)	d(H···A)	d(D···A)	<(DHA)
N1-H1···O2	0.93	2.03	2.950(3)	170.4
N2-H2···O3#2	0.93	2.25	3.057(3)	144.3
O1W-H1WA···O1#3	0.84	2.17	2.993(4)	167.7
O1W-H1WB···O2	0.84	2.03	2.862(4)	171.0
O2W-H2WA···O1W	0.84	2.10	2.909(6)	161.3
O2W-H2WB···O1W#4	0.84	2.15	2.992(6)	178.4

Symmetry transformations used to generate equivalent atoms:

#1 -x+1,-y+1,-z+1 #2 x,y-1,z

#3 -x+1,-y+2, -z+1 #4 -x+1,-y+2,-z

The complex **2,** as illustrated in Figure 3, was obtained by reaction of the macrocycle **L2** and $AgNO_3$ in $MeOH/H_2O$. The coordination environment around the central Ag(II) ion is a square plane with four Ag-N bonds from macrocyclic ligand and two Ag-O bonds from nitrate ions. The silver atom sits on an inversion center. Two weak interactions at the axial sites for the Ag(II) ion have been observed between Ag and O atoms from nitrate ions. The Ag-N distances are in the range of 2.1424(18) – 2.1788(19) Å. The Ag-O distance of 2.8856(19) Å is shorter than that in the complex **1** ([Ag(**L1**)]$(NO_3)_2 \cdot 4H_2O$; Ag-O = 2.923(2) Å). The macrocyclic ligand **L2** contains two cyclohexane rings which are *cis*- fused on the cyclam. As a result, hydrogen bonding interactions are observed between one of the hydrogen atoms connected to C3 and O1 from the nitrate ion and between one of the hydrogen atoms connected to C5 and O3 from the nitrate ion, repectively (C3-H1C3···O1 : d(H···A) = 2.731 Å, <(DHA) = 144.85° ; C5-H1C5···O3 : d(H···A) = 2.559 Å, <(DHA) = 160.09°).

The lattice cell of **2** contains two nitrate ions and two water molecules. The basic unit [Ag(**L2**)]$(NO_3)_2 \cdot 2H_2O$ works as a “metal complex synthon” for the formation of a 1D supramolecular polymer. The 1D chain of **2** is formed through hydrogen bonds between the nitrate ions of basic unit [Ag(**L2**)]$(NO_3)_2 \cdot 2H_2O$ and the lattice water molecules. (Figure 4, Table 4).

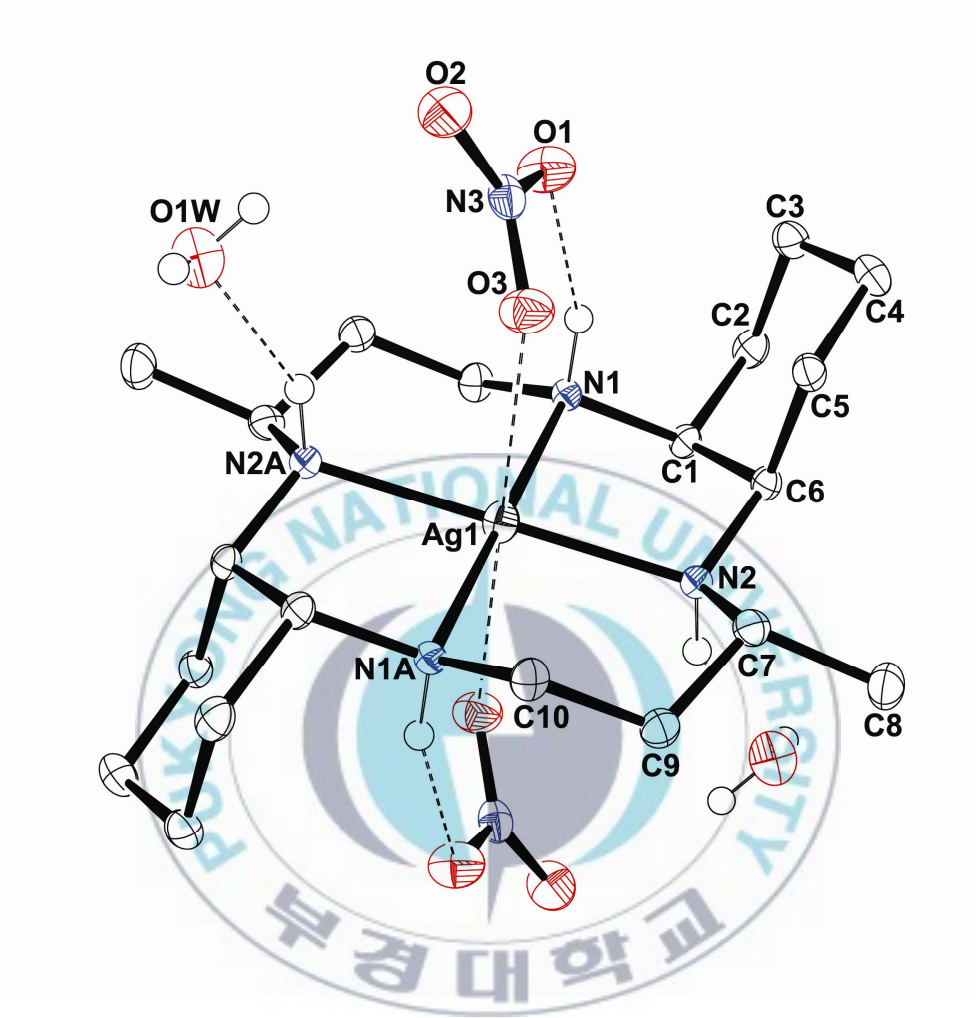

Figure 3. Molecular structure of [Ag(**L2**)]$(NO_3)_2 \cdot 2H_2O$ (**2**) with atom-labeling scheme. Hydrogen atoms other than those participating in hydrogen bonding are omitted for clarity.

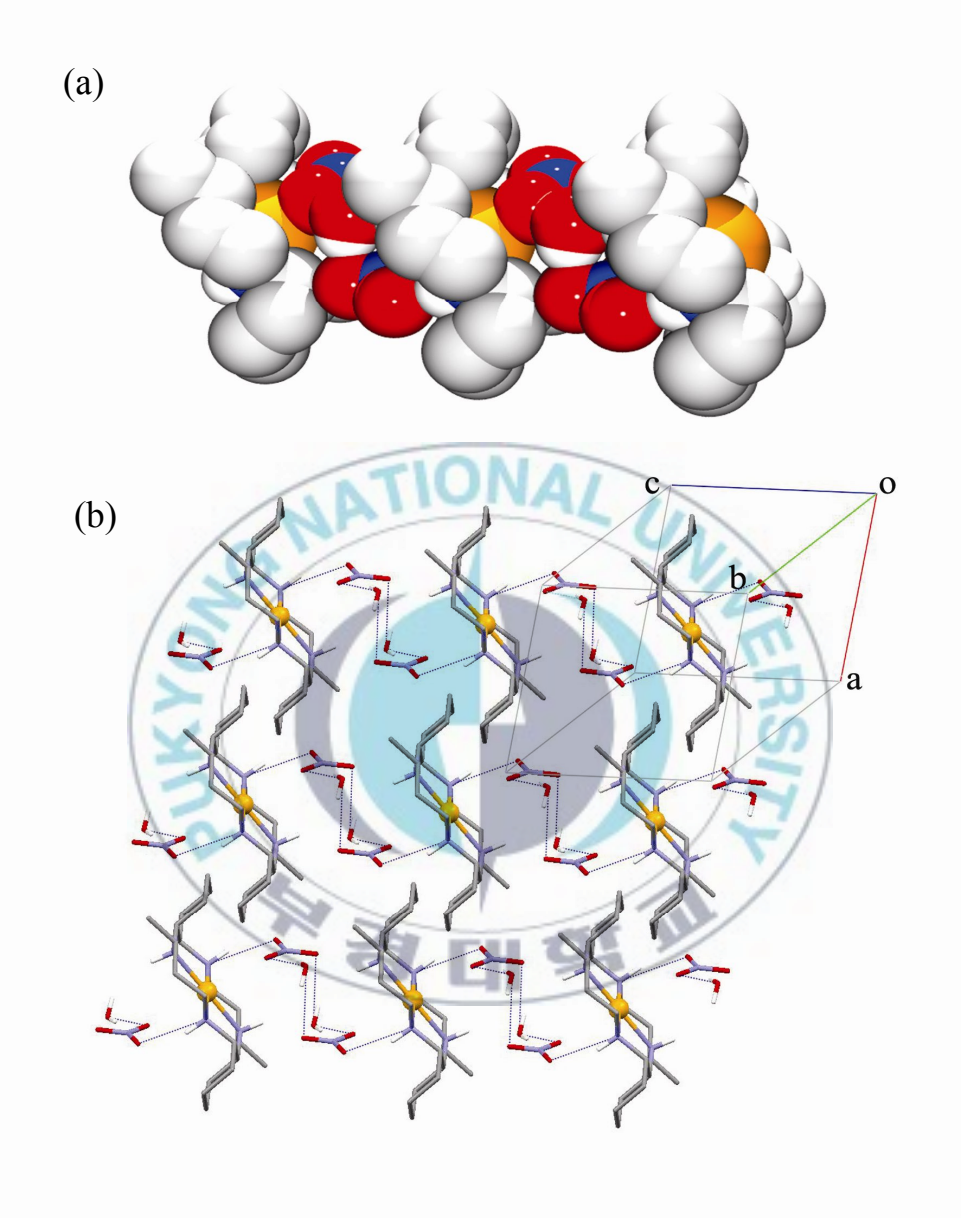

Figure 4. Space-filling (a) and lattice diagram (b) of $\{[Ag(\mathbf{L2})](NO_3)_2 \cdot 2H_2O\}_n$ (**2**) illustrating a 1D supramolecule. Hydrogen atoms are omitted for clarity.

.

Table 4. Selected bond distances (Å) and angles (°) for [Ag(**L2**)]$(NO_3)_2 \cdot 2H_2O$ (**2**)

Ag1-N1	2.1424(18)	Ag1-N2	2.1788(19)
Ag1-O3	2.8856(19)	O1-N3	1.246(3)
O2-N3	1.254(3)	O3-N3	1.257(3)
N1-Ag1-N2	82.44(7)	N1-Ag1-N2#1	97.56(7)
N1-Ag1-O3	86.58(6)	N2-Ag1-O3	97.53(7)
N1#1-Ag1-O3	93.42(6)	N2#1-Ag1-O3	82.47(7)

Symmetry transformations used to generate equivalent atoms:

#1 -x+1,-y+1,-z+1

Table 5. Hydrogen bonds for [Ag(**L2**)]$(NO_3)_2 \cdot 2H_2O$ (**2**) (Å and °)

D-H···A	d(D-H)	d(H···A)	d(D···A)	<(DHA)
N1-H1···O1	0.93	2.13	2.996(3)	155.1
N2-H2···O1W#1	0.93	2.26	3.113(3)	153.1
O1W-H1WA···O2	0.76(4)	2.15(4)	2.886(3)	164(4)
O1W-H1WB···O3#2	0.72(4)	2.29(4)	2.993(3)	166(4)

Symmetry transformations used to generate equivalent atoms:

#1 -x+1,-y+1,-z+1 #2 -x+1,-y+1,-z+2

The complexes contain nusual Ag(II) ion which is stabilized by tetraazamacrocyle **L**. Macrocyclic ligands **L1** and **L2** are the derivatives of the cyclam, which has *trans*- or *cis*- fused cyclohexane rings on the cyclam. The Ag-O bond of complex in **2** is shorter than that in **1**. The 1D silver(II) supramolecular polymer of **1** is formed by various types of hydrogen bonds in which the macrocyclic ligand **L1** contains *trans*-fused cyclohexane rings. In addition to the weak interactions between the Ag(II) ion and the O atoms of the nitrate ions, and the presence of hydrogen bonds between the two sets of pre-organized N-H groups of the macrocyclic ligand and nitrate ions enable the basic unit $[Ag(\mathbf{L1})](NO_3)_2 \cdot 4H_2O$ to result the formation of a 1D supramolecular polymer. Then, the lattice water molecules mediate to interconnect each 1D chain to form the 2D supramolecular sheet. The 1D silver(II) supramolecular polymer of **2** in which the macrocyclic ligand **L2** contains *cis*-fused cyclohexane rings. In addition to the weak interactions between the Ag(II) ion and nitrate ions, lattice water molecules are involved in the formation of a 1D supramolecule.

*Spectroscopic properties and electrochemical analysis for**1** and **2***

The complexes **1** and **2** show the similar spectroscopic properties resulting in the same electron configuration. The microanalysis supported the structure determined by X-ray diffraction studies and the IR spectrum gave evidences for the presence of the macrocyclic ligand and nitrate ions.

The electronic spectra for **1** (λ_{max} = 341 nm in DMF) and **2** (λ_{max} = 346 nm in DMF) (DMF = Dimethylformamide) were that for a d^9 Ag(II) ion. There is an absorption band characteristic for square - planar complex of Ag(II): (Ag(**cyclam**)$^{2+}$ λ_{max} = 350 nm; Ag(**scorpiand**)$^{2+}$ λ_{max} = 376 nm; Ag(**trans-Me$_2$[14]anN$_4$**)$^{2+}$ λ_{max} = 348 nm) [6]. The band was assignable to d-d transition arising from the $b_{2g} \rightarrow b_{1g}$ transition in the field of the ligand under D_{4h} symmetry [18] (Figure 6). Octahedral complexes change their coordination geometries by Jahn-Teller effect ($O_h \rightarrow D_{4h}$). Thus, orbitals including z components are more stable and have lower energy level. As a result, a Ag(II) ion has a d^9 electron configuration as shown in Figure 5.

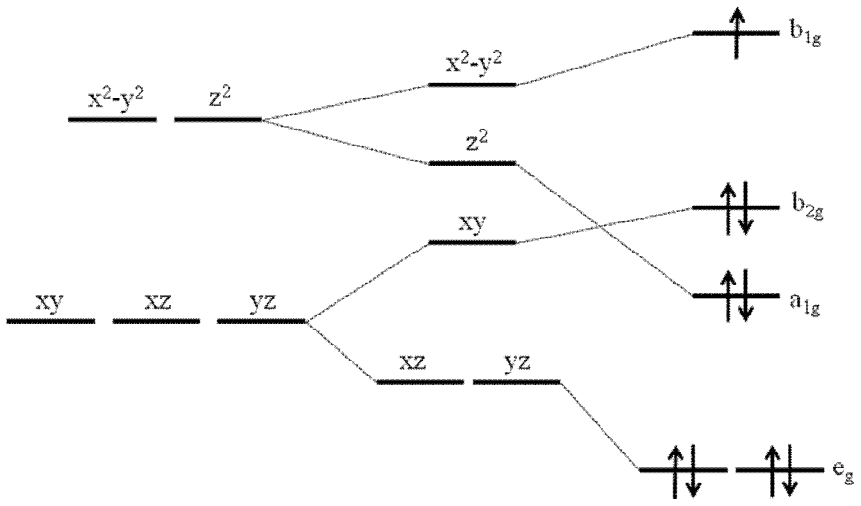

Figure 5. d orbital energy level of octahedral environment (a) d orbital energy level of tetragonal distortion environment (b) d orbital energy level of square – planar environment (c) and d^9 electron configuration.

The ambient temperature powder EPR spectra of **1** and **2** showed axial spectra with principal g-factor values at $g_{\parallel}$ = 2.09695, $g_{\perp}$ = 2.02038 for **1**, $g_{\parallel}$ = 2.10608, $g_{\perp}$ = 2.02195 for **2**. The each spectrum was typical of d^9 square planar configuration around the Ag(II) ion (^{107,109}Ag, *I*-1/2). The hyperfine structure due to the ^{14}N nuclei(*I*-1) was not observed [7] (Figure 7) .

The cyclic voltammogram was similar to that of [Ag(**cyclam**)]$^{2+}$, but not the same, especially for the redox behavior in the positive potential region [9].

Therefore, the interpretation of the cyclic voltammogram for **1** is quite different from that of [Ag(**cyclam**)]$^{2+}$. The cyclic voltammogram of the complex **1** is quite similar but reduction peak is somewhat different. The reduction peak A in Figure 8 can be assigned to 2e reduction of [Ag(**L1**)]$^{2+}$ to Ag and **L1** *via* the [Ag(**L1**)]$^{1+}$ intermediate. The small oxidation shoulder B is presumed to be due to the oxidation of the remained [Ag(**L**)]$^{1+}$ intermediate. The next oxidation peak C is associated with the oxidation of deposited Ag to Ag(I). The peak D that was not appeared in the first scan can be assigned to the reduction of Ag(I) to Ag. Since the amount of deposited Ag was increased due to the free Ag(I) as well as [Ag(**L1**)]$^{2+}$, the reduction peak C increased in the second scan. In Figure 9 the oxidation of [Ag(**L1**)]$^{2+}$ to [Ag(**L1**)]$^{3+}$ is shown as a peak at +0.45 V (E), but the corresponding reduction is not shown. This indicates that the oxidation of [Ag(**L1**)]$^{2+}$ is an irreversible process and [Ag(**L1**)]$^{3+}$ is unstable. After positive scan up to +1.0V, the Ag/Ag^{+} redox peaks(C and D) increased as shown in Figure 8 and 9. This could be ascribed to Ag(I) formed from the decomposed [Ag(**L1**)]$^{3+}$.

The cyclic voltammogram of complex **2** is quite similar with that of complex **1** but the reduction feature is somewhat different. The reduction peaks, A and B in Figure 10 can be assigned to the reduction of [Ag(**L2**)]$^{2+}$ to [Ag(**L2**)]$^{1+}$ and [Ag(**L2**)]$^{1+}$ to Ag and **L2,** respectively, as shown in [Ag(**cyclam**)]$^{2+}$ [9]. In the first scan of Figure 11, a clear oxidation peak E is shown at the potential of +0.59

V and the corresponding reduction peak was very small relative to the oxidation one. The oxidation peak E is decreased in the second scan and stabilized after the second scan. In the case of $[Ag(\mathbf{L1})]^{2+}$ two separate reductions were not observed on the scan 50 mV/s. This implies that $[Ag(\mathbf{L2})]^{1+}$ is more stable than $[Ag(\mathbf{L1})]^{1+}$. The oxidation shoulder C can be presumably due to the oxidation of remained $[Ag(\mathbf{L2})]^{1+}$. The next sharp oxidation peak D is due to the oxidation of deposited Ag to Ag^{+}. Interestingly, the reduction of Ag^{+} that was observed for $[Ag(\mathbf{L2})]^{2+}$ was not observed for $[Ag(\mathbf{L1})]^{2+}$.

As the complexes **1** and **2** have the same electron configuration the spectroscopic properties for **1** and **2** are similar. The UV/vis spectra for **1** and **2** are expected for d^9 silver(II) ions in square - planar environment. The EPR spectra for **1** and **2** exhibited typical d^9 ions in an axially distorted ligand field. The electrochemical behaviors for **1** and **2** showed quite similar but reduction feature is somewhat different.

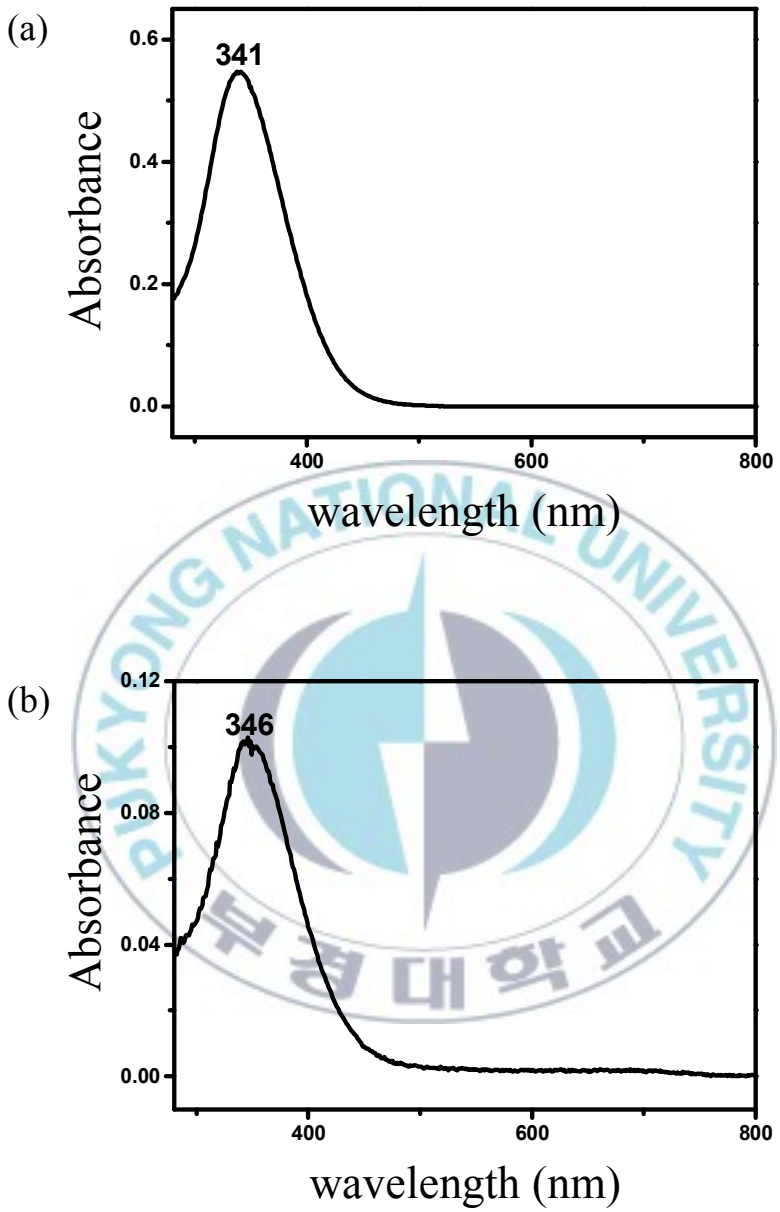

Figure 6. UV/vis spectra of (a) [Ag(**L1**)]$(NO_3)_2 \cdot 4H_2O$ (**1**) and (b) [Ag(**L2**)]$(NO_3)_2 \cdot 2H_2O$ (**2**).

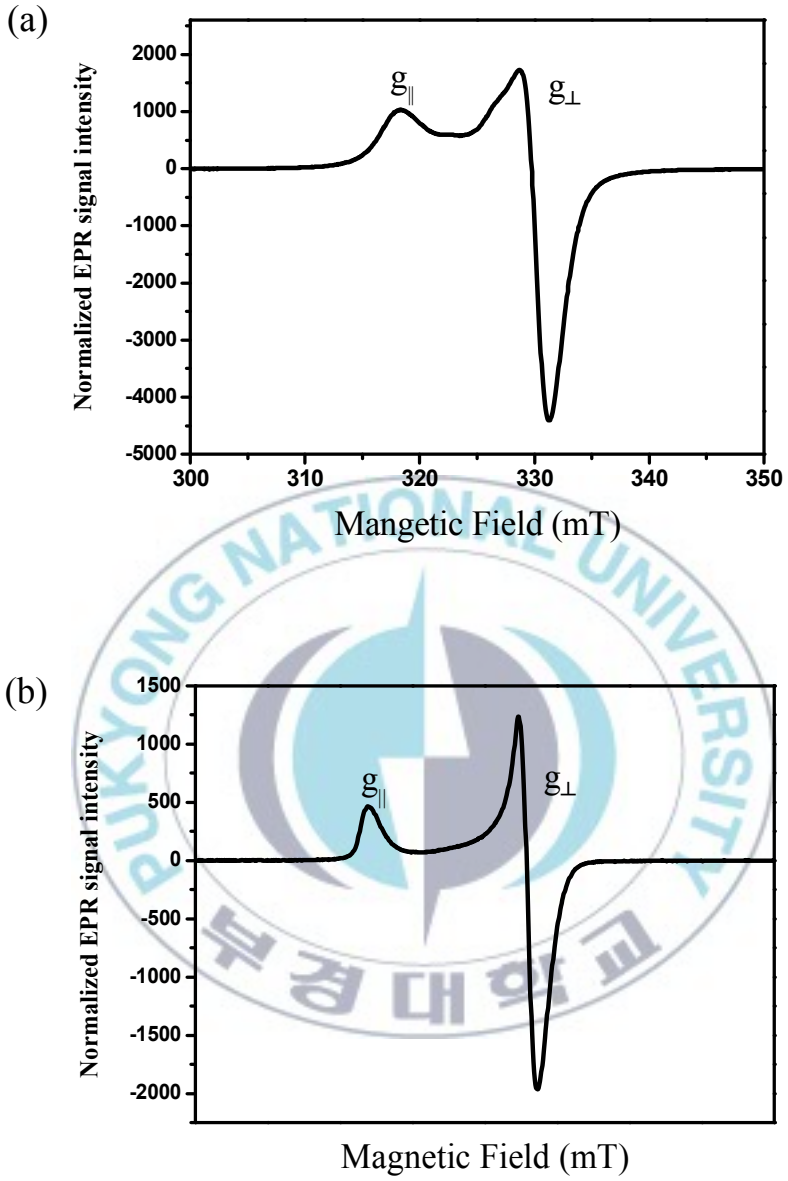

Figure 7. Powder EPR spectra of (a) [Ag(**L1**)]$(NO_3)_2 \cdot 4H_2O$ (**1**) ($g_{\|}$ = 2.09695, $g_{\perp}$ = 2.02038) and (b) [Ag(**L2**)]$(NO_3)_2 \cdot 2H_2O$ (**2**) ($g_{\|}$ = 2.10608, $g_{\perp}$ = 2.02195) at ambient temperature.

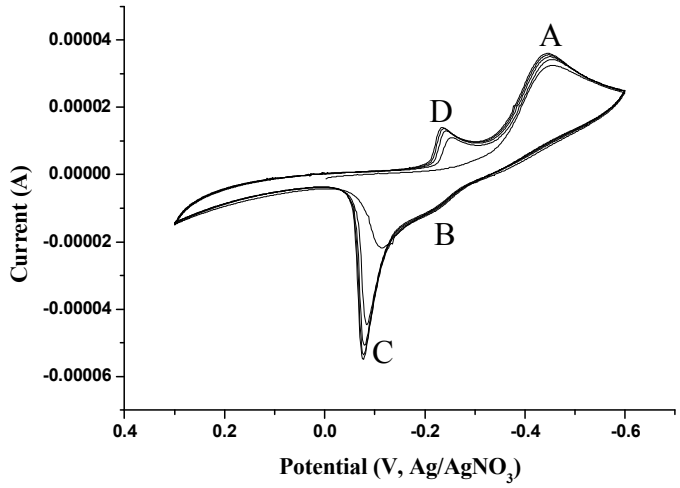

Figure 8. Cyclic voltammogram of **1** in the potential window between –0.6 and +0.3 V vs $Ag/AgNO_3$ (v = 50 mV s^{-1}, on Pt in 0.1M TEAP), the concentration of **1** was not determined.

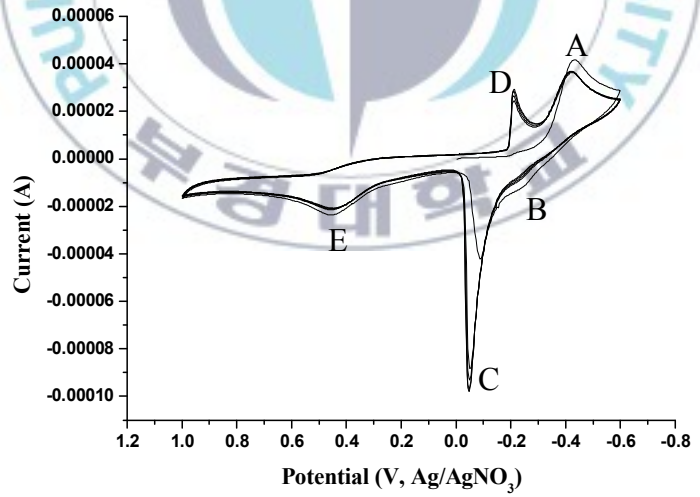

Figure 9. Cyclic voltammogram of **1** in the potential window between –0.6 and +1.0 V vs $Ag/AgNO_3$ (v = 50 mV s^{-1}, on Pt in 0.1M TEAP), the concentration of **1** was not determined.

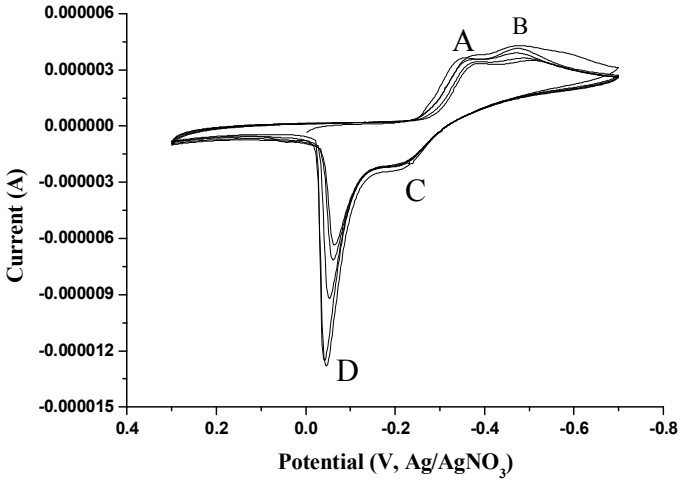

Figure 10. Cyclic voltammogram of **2** in the potential window between –0.7 and +0.3 V vs $Ag/AgNO_3$ (v = 50 mV s^{-1}, on Pt in 0.1M TEAP), the concentration of **2** was not determined.

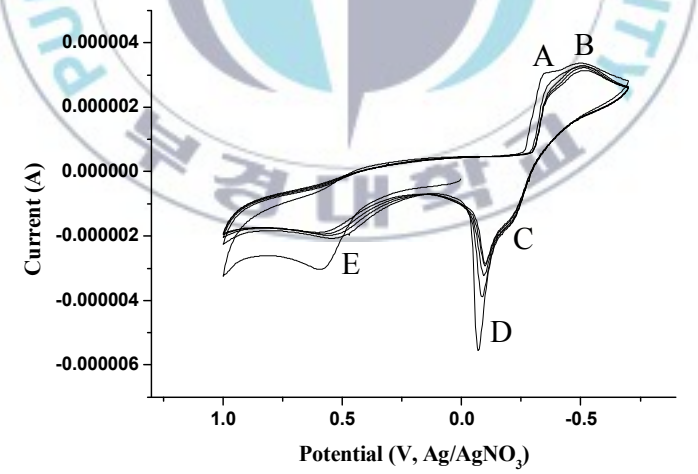

Figure 11. Cyclic voltammogram of **2** in the potential window between –0.7 and +1.0 V vs $Ag/AgNO_3$ (v = 50 mV s^{-1}, on Pt in 0.1M TEAP), the concentration of **2** was not determined.

References

[1] S. Kitagawa, R. Kitaura, S. -I. Noro, Angew. Chem. Int. Ed. 43 (2004) 2334.

[2] C. Janiak, Dalton Trans. (2003) 2781.

[3] Y.-Y. Yang, W.-T. Wong, Chem. Commun. (2002) 2716.

[4] M. P. Suh, Y. E. Cheon, E. Y. Lee, Coord. Chem. Rev. 252 (2008) 1007.

[5] H. Park, J. C. Kim, A. J. Lough, B. M. Lee, Inorg. Chem. Commun. 10 (2007) 303.

[6] D. Sroczyński, A. Grzejdziak, J. Inclusion Phenom. Macrocyclic Chem. 42 (2002) 99.

[7] M. Ali, A. I. Shames, S. Gangopadhyay, B. Saha, D. Meyerstein, Transition Met. Chem. 29 (2004) 463.

[8] M. Pesavento, A. Profumo, T. Soldi, L. Fabbrizzi, Inorg. Chem. 24 (1985) 3873.

[9] I. J. Clark, J. M_{AC}B. Harrowfield, Inorg. Chem. 23 (1984) 3740.

[10] E. K. Barefield, M. T. Mocella, Inorg. Chem. 12 (1973) 2829.

[11] M. O. Kestner, A. L. Allred, J. Am. Chem. Soc. 94 (1972) 7189.

[12] K. B. Mertes, Inorg. Chem. 17 (1978) 49.

[13] H. N. Po, E. Brinkman, R. J. Doedens, Acta Cryst. C47 (1991) 2310.

[14] S.-G. Kang, J. K. Kweon, S.-K. Jung, Bull. Korean Chem. Soc. 12 (1991) 483.

[15] J. A. Kim, H. Park, J. C. Kim, A. J. Lough, S. Y. Pyun, J. Roh, B. M. Lee, Inog. Chim. Acta. 361 (2008) 2087.

[16] J. C. Kim, J. Cho, H. Kim, A. J. Lough, Chem. Commun. (2004) 1796.

[17] S.-G. Kang, M.-S. Kim, D. Whang, K. Kim, J. Chem. Soc. Dalton Trans. (1994) 853.

[18] A. Grzejdziak, Monatsh. Chem. 125 (1994) 107.

[19] T. Ito, H. Ito, K. Toriumi, Chem. Lett. (1981) 1101.

[20] Z. Otwinowski, W. Minor, In *Methods in Enzymology, Macromolecular Crystallography, Part* A;C. W. Carter, R. M. Sweet, Eds.; Academic Press: London, 276 (1997) pp 307.

[21] G. M. Sheldrick, SHELXTL\PC V6.1, Bruker Analytical X-ray Systems, Madison, WI, 2001.

[22] K. R. Adam, I. M. Atkinson, L. F. Lindoy, Inorg. Chem. 36 (1997) 480.

.

Acknowledgments

I would like to extend my special appreciation to my advisor, Prof. Ju Chang Kim, whose academic guidance made my life as well as my study a precious experience.

I would also like to thank Prof. Sang Yong Pyun and Prof. Yong-Cheol Kang for their time and comments for this thesis. I am appreciative of the guidance and help of other faculty members during the stay at department of chemistry at PKNU. In addition, I am grateful to Prof. Young Il Kim for obtaining electrochemical data.

I am grateful for their friendships to Sol Han, Jin Suk Kwag, Taehyung Kim, Chungsik Jang in Molecular Design Lab. Finally I am greatly thankful to my parents for their constant supports and thoughtfulness throughout my whole life.